Mine Water and the Environment (2024) 43:326–339
https://doi.org/10.1007/s10230-024-00983-5

TECHNICAL ARTICLE

Assessment of Bitumen-Influenced Aquifers in Southwestern Iran Based on Groundwater Geochemistry and Stable Isotopes Characteristics

Narges Bayat[1] · Farshad Alijani[1] · HamidReza Nassery[1]

Received: 3 February 2024 / Accepted: 3 May 2024 / Published online: 16 May 2024

Abstract
Iran is situated in a region with natural bitumen deposits and bitumen mines. This study compared the hydrogeochemical and isotopic composition of groundwater contaminated by abandoned bitumen mines (GCBM) with the deep formation water of oil reservoirs (FWOR). The GCBM was found to be dominated by Ca^{2+}, Na^{+}, SO_4^{2-}, and Cl^{-}, and is typically characterized by Ca–SO_4 type water, in contrast to the Na–Cl type in the FWOR. The δ^2H_{H2O} and $\delta^{18}O_{H2O}$ isotopes were valuable tools to distinguish the groundwater sources, as the isotope signatures of GCBM and FWOR samples are markedly different. Ionic ratio diagrams, such as Na^{2+} vs. Cl^{-}, Ca^{2+} vs. Cl^{-}, and SO_4^{2-} vs. Cl^{-}, indicate that the groundwater chemistry in the study area is mainly influenced by gypsum and carbonate dissolution due to mining. The concentration of total petroleum hydrocarbons (TPH) ranged from 26.3 to 19,670 µg/L in the GCBM samples. This study confirmed unacceptable levels of groundwater contamination by TPH caused by seepage from abandoned bitumen mines and established a framework for future groundwater remediation efforts in the study area.

Keywords Abandoned bitumen mine · Groundwater hydrochemistry · Formation water · Southwest Iran

Introduction

Bitumen, a dense mixture of diverse hydrocarbon compounds, is formed by the gradual degradation of lighter crude oil (Brown et al. 2017; Speight 2005; Stoyanovich et al. 2019). Heavy oil and bitumen have great importance in global reserves of hydrocarbon. Bitumen is extracted by surface mining or in situ methods in various regions around the world. The nations of Canada, the United States of America, Venezuela, Russia, Iraq, and Iran all posses large quantities of this precious substance. The Athabasca oil sands, the largest of three oil sands reserves in Alberta, represent one of the world's largest natural bitumen deposits (Finkel 2018). These deposits, responsible for nearly 3 million barrels per day of production in 2019 (Alberta Energy Regulator 2021; Vander Meulen et al. 2023), are predominantly extracted by surface mining, which has led to major land and ecosystem disruption. The disturbed area reached ≈3200 km^2 by 2018, directly attributed to energy-related activities (Alberta Biodiversity Monitoring Institute 2018). Other notable reserves can be found in Venezuela, Russia, and Kazakhstan (Finkel 2018). Proven reserves of bitumen make up around 100 billion barrels, with total natural bitumen reserves worldwide estimated at 39.694×10^9 m^3 (249.67 Gbbl) (Attanasi and Meyer 2010; Korosi et al. 2016). After Canada and the United States, Iran is recognized as having the largest natural bitumen deposits. Indeed, more than 15% of the world's valuable bituminous mineral is found in southwest Iran (Rahimi et al. 2020), and much of it is being mined, especially in the mountainous Zagros area (Ameri et al. 2011; Maadanara consulting engineering 1996; Maadankave consulting engineering 1999).

Two primary methods are used to extract bitumen: surface mining, which targets oil sand deposits within the top 0–60 m of the Earth's surface, representing only 20% of the proven reserves, and in situ methods, which are used to recover the remaining 80% (Abdelfatah et al. 2018). In

✉ Farshad Alijani
f_alijani@sbu.ac.ir

[1] Department of Minerals and Groundwater Resources, Faculty of Earth Sciences, Shahid Beheshti University, Evin Ave, Tehran, Iran

cases where there is insufficient cap rock above the bitumen-bearing tar-sand horizon, bitumen can migrate upward toward the water table, resulting in groundwater contamination with bitumen-sourced pollutants, including polycyclic aromatic hydrocarbons (Adeyemi et al. 2013). These hydrocarbon contaminants have been observed to migrate and disperse within the surface and near-surface environment through structural and lithological pathways (Ola and Olabode 2017).

Since the 1960s, persistent concerns have arisen regarding the potential environmental effects of regional mining and upgrading activities on water quality and the health of aquatic ecosystems (Gosselin et al. 2010; Kelly et al. 2010; Wasiuta et al. 2019). A particular group of pollutants, known as naphthenic acids (NAs), which are a subgroup of bitumen-derived dissolved organic compounds with the chemical formula $C_nH_{2n+z}O_2$, has been identified as a potentially toxic mixture (Brown and Ulrich 2015). In addition, the production of crude oil and gas from oil wells typically brings forth what is known as "formation waters" or "oilfield brines" from the oil reservoir (FWOR). These waters originate either from within the geological formation itself (connate) or from recent precipitation (meteoric), as defined by White (1957). Connate water has been isolated from the hydrological cycle for extensive geological periods, contrasting with meteoric water which is comparatively more recent in the cycle, resulting in distinct chemical compositions (Dickey 1966). These formation waters often contain petroleum hydrocarbons that may occasionally infiltrate groundwater aquifers through karstic fractures or conduits.

The present study investigated the environmental effects of abandoned bitumen mines on southwestern Iran's groundwater resources using hydrogeochemical and isotopic analyses. The objectives of this study were to: (1) define the hydrogeochemical and isotopic characteristics of the groundwater contaminated by the abandoned bitumen mines (GCBM), (2) compare them with the FWOR, and (3) evaluate the impact of bitumen mines on the TPH levels in GCBM.

Materials and Methods

Study Area

This study was carried out in the geographical coordinates ranging from 30° 45′ N to 33° 05′ N for latitude and from 47° 15′ E to 50° 35′ E for longitude, southwest Iran, covering an area of 48,000 km^2 (Fig. 1). The study area experiences a distinct climatic pattern characterized by scorching high temperatures exceeding 45 °C during the dry season, while lower temperatures are observed during the rainy season. As a result of the arid climate prevalent in the area, the average annual precipitation totals 360 mm, predominantly occurring in autumn and winter. The area is crossed by numerous rivers, including the Karun and Karkheh Rivers.

Geological Setting

The collision of the Central Iran and Arabian tectonic plates during the Cretaceous era formed the Zagros Foreland Basin (ZFB) on the southern side of the Tethyan Ocean (Berberian and King 1981; Sherkati et al. 2006) (Fig. 1). The ZFB extends from southwestern Iran to Turkey. The modern form of this convergent basin is the Iranian Zagros fold-thrust belt (ZFTB), which can be subdivided into different tectonostratigraphic domains. The ZFTB and its Foreland Basin offer ideal conditions for the generation and accumulation of hydrocarbons, earning it a global reputation as a petroleum-rich region. A substantial portion of the world's oil reserves, over 8%, is concentrated in the Dezful Embayment, a 60,000 km^2 depression within the ZFTB, in southwest Iran (Bordenave and Burwood 1995), where the main deposits consist of shallow and deep carbonates (Illam-Sarvak and Asmari Formation) with evaporites (Gachsaran Formation). The study area is situated in this area.

In the Zagros Basin, the Illam-Sarvak Formation from the Upper Cretaceous carbonates serve as the best example of paleokarstic reservoirs. These formations trap large volumes of hydrocarbons within dissolved carbonate units (Ismail et al. 2021; Mehrabi et al. 2023). The Asmari Formation is the youngest carbonate reservoir rock in the Zagros basin, and is a notable source for oil and bitumen in southeastern Iran (Noorian et al. 2022). The Asmari Formation is overlain by the lower Miocene Gachsaran Formation, which plays a crucial role as a seal for hydrocarbon reservoirs in one of the world's most prolific hydrocarbon habitats (Bahroudi and Koyi 2004; Stöcklin 1968). The Gachsaran Formation contains mostly evaporites; it also contains marls, limestones, and shales (Bahroudi and Koyi 2004). The hydrocarbon substances in bitumen, initially bound in sediments, undergo diffusion processes, leaching by groundwater or hydrothermal solutions, and maturation (polymerization) in vein fillings, ultimately forming solid bitumen.

In the study area, bitumen was observed seeping to the surface within the alluvial plain sands, appearing as a predominantly dark-brownish substance (Fig. 2). Surface and groundwater in the area displayed signs of contamination from these bitumen seepages, causing the water to be dark brown in color (Fig. 2).

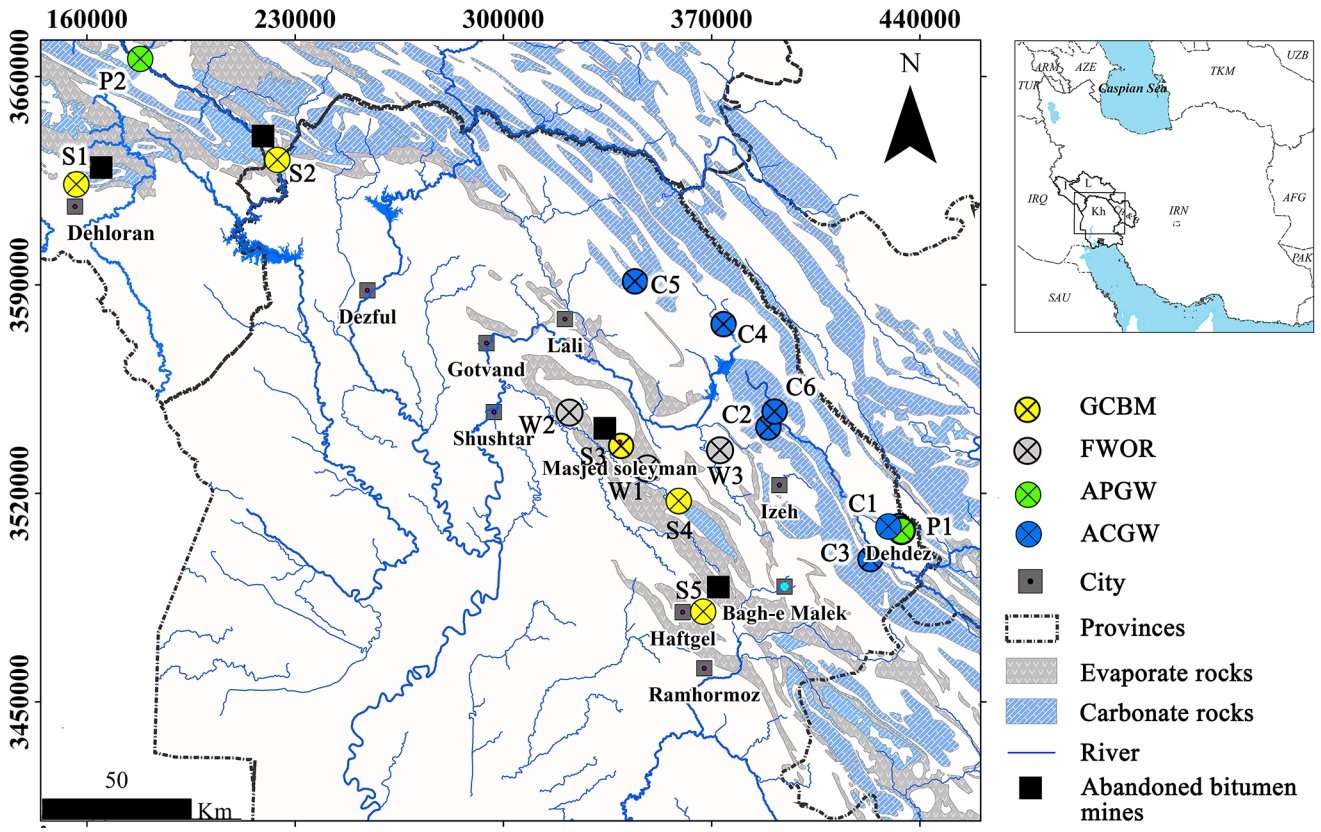

Fig. 1 Geological map and location of the GCBM, FWOR, and APGW sampling points of this study and ACGW (Farhadi et al. 2023). The sampling points were located near the bitumen seeps. Samples from this study included GCBM (groundwater contaminated by abandoned bitumen mines), FWOR (formation water of oil reservoirs), APGW (Asmari polluted groundwater), and ACGW (carbonate clean groundwater from Farhadi et al. (2023). Evaporite rocks (Gachsaran), carbonate rocks (Asmari and Illam -Sarvak)

Mines Site Locations

Natural bitumen in southwestern Iran is recognized as a mineral resource, and has been mined for many decades. Abandoned bitumen mines are located in the extreme northern part of the study area. Crude oil has been able to migrate from the abundant, relatively shallow oil resources in southern Iran to the surface through fractures and are presumably the source of the bitumen. The mines investigated in this study (Dehloran, Pol-e-Zal, Mamatin, and C Brench) are categorized as abandoned mines, having been actively mined ≈ 50 to 100 years ago. The sampling points were located adjacent to bitumen seeps (Fig. 1).

The Dehloran mine, located 7 km east of Dehloran town in Ilam province, is situated in the southern part of the Siah kuh anticline within the Asmari formation. Bitumen mineralization is present in this region. The S1 spring is located ≈ 20 m southwest of the Dehloran mine, at an elevation ≈ 35 m lower. Additionally, there are local bitumen outcrops surrounding the S1 spring. Moving on to the Pol-e-Zal mine, situated 70 km northwest of Dezful town in Lorestan province, its bitumen mineralization is found in the southeast of the Kabir kuh anticline within the Asmari formation. The S2 spring is positioned ≈ 1.5 km southeast of the Pol-e-Zal mine, ≈ 350 m below the mine. Local bitumen outcrops are also present around the S2 spring (Fig. 2).

The C Brench mine, located 15 km east of Masjed Solayman town in Khuzestan province, features natural bitumen mineralization southeast of the Kabir kuh anticline within the Gachsaran formation. The S3 spring, located ≈ 600 m southeast of the C Brench mine, and ≈ 75 m below the mine. Additionally, there are local bitumen outcrops around the S3 spring. Finally, the Mamatin mine, situated 25 km northeast of Ramhormoz town in Khuzestan province, exhibits natural bitumen mineralization southwest of the Mamatin village within the Gachsaran formation. The S5 spring, positioned about 50 m southwest of the Mamatin mine, is ≈ 3 below it. Local bitumen outcrops surround the S5 spring as well (Fig. 2).

Sampling and Analyses

Five groundwater samples contaminated by the abandoned bitumen mines, two hydrocarbon polluted groundwater

Fig. 2 The seepage of bitumen and bitumen-driver contaminants in the studied groundwater: a, b, and c) spring S5; d, e) spring S1; f, g, h, and i) spring S2

Table 1 The characteristics of sampling waters in study area

Samples			Coordinates (Zone, UTM X, UTM Y)	Elevation	T (°C)	Maximum discharge (L/sec)
Group	Name	Sample ID				
GCBM	Dehloran	S1	38R 718,946 3,620,221	265	29.5	3
	Pol-e-Zal	S2	39R 224,003 3,631,995	287	24	100
	C Brench	S3	39R 339,545 3,535,919	249	24	1
	Garu	S4	39R 358,933 3,517,431	401	26	80
	Mamatin	S5	39R 380,982 3,466,098	316	29	0.5
FWOR	Masjed Soleyman	W1	39R 348,294 3,528,393	447	80	Formation water well (Depth = 3000)
	Zilaei	W2	39R 322,197 3,547,127	472	50	Formation water well (Depth = 2540)
	Marghab	W3	39R 372,795 3,534,496	576	80	Formation water well (Depth = 3000)
APGW	Dehdez	P1	39R 434,446 3,507,027	1553	19	well
	Tang- Fani	P2	38R 757,996 3,657,711	569	24	3

samples (APGW), and three samples of deep formation water were collected during different seasons: Feb-2022 (GCBM and APGW), Mar-2022 (FWOR) during the wet season, and Aug-2021 (GCBM, APGW, and FWOR) (Table 1). The APGW samples comprise two hydrocarbon polluted samples from carbonate aquifers (P1-P2) and the ACGW including six clean karst spring waters (C1-C6) from previous literature (Farhadi et al. 2023) were used to compare the GCBM and FWOR. A combination of newly collected and historical data was used to determine the effect of the abandoned bitumen mines on groundwater. For FWOR sampling, the Wireline bottomhole travers truck was used to sample water observation wells in the oil reservoirs. In this method, the sampling tool is sent to the desired depth using a wireline slickline and retained at that depth for one hour. Subsequently, the tool is returned to the surface, and the sampled contents are emptied into specialized sampling containers.

The distribution of the sampling locations can be observed in Fig. 1. Prior to sampling, the polyethylene bottles were

thoroughly rinsed two to three times with ultrapure water. Handheld portable devices were used to directly measure pH levels, total dissolved solids (TDS), and temperatures. The concentrations of Ca^{2+}, Mg^{2+}, Na^{+}, and K^{+} were determined using a Dionex 1500 ion chromatography (ICS), SO_4^{2-}, and Cl^{-} were determined using a Dionex 2100 ICS, and HCO_3^{-} values were measured by acid-base titration in Hydroisotop GmbH laboratory (Germany). The analytical precision error of the Dionex 1500 and 2100 ICS instruments is < 5%. Blank and duplicate samples were employed to ensure data quality. The accuracy of the laboratory data analyses was checked using the charge balance error percentage (% CBE) in Eq. (1).

$$\%\mathrm{CBE} = \left(\sum_i^m c_e^+ - \sum_i^m c_e^-\right) \Big/ \left(\sum_i^m c_e^+ + \sum_i^m c_e^-\right) \quad (1)$$

where c_e^{i+} and c_e^{i-} refer to the concentrations of specific cations and anions, respectively. The absolute values of % CBE for all samples were consistently < 5%, indicating the reliability of the test data.

Stable isotopes of hydrogen (H) and oxygen (O) in water serve as valuable indicators for determining the source of water and its movement, and are commonly used in hydrological research (Barnes and Allison 1988; Li et al. 2017). Samples for stable isotopes ($\delta^{18}O_{H2O}$, $\delta^{2}H_{H2O}$) analysis were filtered through 0.45 µm membranes and collected in 50 mL PET bottles which had been carefully rinsed before sampling. Stable isotopes ($\delta^{18}O_{H2O}$, $\delta^{2}H_{H2O}$) of water samples were determined with the Picarro Cavity-Ringdown Spectrometer L2130-I in the Hydroisotop GmbH laboratory. Accuracy of the determination of isotope composition for hydrogen and oxygen are ± 1.5‰ for $\delta^{2}H_{H2O}$ and ± 0.15‰ $\delta^{18}O_{H2O}$ values. Unfiltered samples for TPH concentration analysis were collected in 50 mL amber glass bottles, then analyzed using an Agilent 7890B/5977A gas chromatography mass spectrometer (GC/MS) in Zanjan University (Iran).

A comprehensive understanding of hydrogeochemical processes and the sources of pollutants, coupled with regular water resource monitoring, plays a crucial role in the effective and sustainable management of water resources worldwide (Tiwari and Singh 2014; Tiwari et al. 2019). Traditional hydrogeochemical methods are valuable for characterizing water types and assessing the processes governing solute acquisition, influencing water chemistry, and determining factors contributing to aquifer quality deterioration (Abu-alnaeem et al. 2018). During bitumen migration to the surface, different effects have been observed on groundwater resources, which we investigated from the perspective of hydrogeochemistry and water isotopes.

In the region, the GCBM and FWOR undergo rapid transformations. To comprehend the hydrochemical evolution of regional waters, it is essential to have a clear understanding of the sources and supplies of the GCBM and FWOR. In this particular study, hydrogeochemical methods, including the Piper trilinear and Ionic ratio diagrams, were used to identify water types, assess ion exchange processes, analyze water-rock interactions, determine the origin of salinity, and evaluate pollution in aquifers affected by abandoned bitumen mines in southwest Iran. Additional published data (Farhadi et al. 2023) from clean karst groundwater samples (ACGW) and two samples of groundwater polluted with TPH from the Asmari formation (APGW) were added to compare with GCBM.

Results

Hydrogeochemistry

A statistical analysis of the physical and chemical characteristics of various types of water bodies is shown in Table 2. The pH values in these two different types of water bodies varied markedly, leaning towards neutral in the GCBM samples to a slightly acidic trend in the FWOR samples. GCBM exhibits an electrical conductivity (EC) range of 1490 to 14,140 µs/cm, with a mean value of 5561 µs/cm. FWOR, on the other hand, falls within the EC range of 1576 to 241,000 µs/cm, with a mean of 124,186 µs/cm. This suggests that GCBM may be influenced by factors such as geological conditions, aquifer media, and the presence of bitumen seeps. Ca^{2+} and Na^{+} are the predominant cations in GCBM and FWOR samples. In contrast, Cl^{-} is the dominant anion in FWOR, while GCBM samples are predominantly characterized by SO_4^{2-} and HCO_3^{-}.

Descriptive statistics of chemical components in ACGW and APGW samples are shown in Table 3. The pH values of ACGW ranged from 7.0 to 7.9, with a mean value of 7.4, which demonstrates that the groundwater environment was slightly alkaline. As shown in Table 3, cation composition was dominated by Ca^{2+}, followed by Mg^{2+}, Na^{+}, and K^{+}. The anions were mainly HCO_3^{-}, followed by SO_4^{2-} and Cl^{-}. Table 3 shows the average major ions for ACGW and APGW samples and clearly, the uncontaminated samples have lower ionic concentrations than the GCBM and FWOR samples.

The interaction between water and rock in the study area is the most important hydrogeochemical process controlling water chemistry (Zhang et al. 2022a, b). The chemical composition of GCBM is primarily governed by the dissolution of the carbonate rocks in the hydrocarbon reservoir. In contrast, the FWOR exhibits a distribution pattern that

Table 2 Statistical summary of the physical, chemical, and isotopic data of GCBM and FWOR samples in dry and wet season

Parameter	Unit	Wet and dry season (GCBM)				Wet and dry season (FWOR)			
		Min	Mean	Max	SD	Min	Mean	Max	SD
pH		7.2	7.4	7.6	0.2	3.9	6.3	7.0	1.1
EC	µs cm^{-1}	1490	5561.5	14,140	4456.3	1576	124,186	241,000	11,4270
Na^+	mg L^{-1}	69	612.4	1700	582.2	170	44,071.7	95,000	40,439.7
K^+	mg L^{-1}	2	64.6	500	154	3.4	473.3	1600	601.8
Ca^{2+}	mg L^{-1}	150	412.2	990	274.1	97	4414.5	9900	4321.3
Mg^{2+}	mg L^{-1}	42	315.7	2200	666.7	23	1436.3	3600	1549.1
HCO_3^-	mg L^{-1}	169	656.7	2400	663.2	8.48	75.9	130	39.6
Cl^-	mg L^{-1}	82	867.3	2700	3250.3	430	81,210	180,000	75,835.9
SO_4^{2-}	mg L^{-1}	21	1942.3	11,000	924.6	2.2	659.5	1400	516.2
SI calcite		0.3	0.9	1.5	0. 5	-4.3	-0.7	0.6	1.7
SI dolomite		0.1	1.6	3.6	1.1	-8.9	-1.57	1.2	3.5
SI gypsum		-2.2	-0.6	0.3	0.7	-3.2	-1.1	-0.1	1.2
δ^2H–H_2O	‰V-SMOW	-18.8	-12.5	-1.9	5.2	-19.6	-9.6	18.4	15.3
$\delta^{18}O$–H_2O	‰V-SMOW	-4.9	-3.8	-2.2	0.8	-4.4	2.3	7.7	5.4

Table 3 Statistical summary of the physical and chemical data of ACGW (Farhadi et al. 2023) and APGW samples in dry and wet seasons)

Parameter	Unit	Wet and dry season (ACGW)				Wet season (APGW)			
		Min	Mean	Max	SD	Min	Mean	Max	SD
pH		7.0	7.4	7.9	0.3	7.3	7.4	7.5	0.1
T	°C	24.1	24.5	25	0.3	24	24.3	24.6	0.3
EC	µs cm^{-1}	268	425	1008	186.1	579	795	1012	216.5
Na^+	mg L^{-1}	0.2	10.7	85.1	22.7	4.1	14.1	24	9.95
K^+	mg L^{-1}	0.4	0.7	2.0	0.5	1.2	1.3	1.4	0.1
Ca^{2+}	mg L^{-1}	32.9	60.4	90.0	17.7	70	77	84.0	7.0
Mg^{2+}	mg L^{-1}	5.0	12.5	20.8	5.1	30	45.5	61.0	15.5
HCO_3^-	mg L^{-1}	151.9	215.4	296.6	40.7	258	416.5	575	158.5
Cl^-	mg L^{-1}	1.1	15.5	124.1	33.2	4.9	14.5	24	9.6
SO_4^{2-}	mg L^{-1}	3.4	27.9	113.8	35.0	0.5	44.7	89	44.2
SI calcite		-0.3	0.1	0.5	0.3	0.3	0.35	0.4	0.1
SI dolomite		-1.1	-0.1	0.8	0.6	0.5	0.8	1	0.2
SI gypsum		-3.2	-2.4	-1.5	0.5	-3.9	-2.8	-1.7	1.1

is close in composition to the evaporite. The Piper diagram (Piper 1944) demonstrates that the three dominant water facies present are the Ca^-, and HCO_3 in ACGW and APGW, and Ca-SO_4 and Na-Cl in GCBM and FWOR, respectively (Fig. 3). Specifically, the S3 groundwater sample is dominated by Ca-HCO_3 in the dry season (Fig. 3a), which aligns with the typical composition found in carbonate environments, as indicated by previous studies on the geochemistry of carbonate aquifers (Zhang et al. 2016).

Variations in the concentration of major ions, total dissolved ions (TDI), and EC for GCBM and FWOR samples in August 2021 and February 2022 are plotted in Fig. 4. Ionic diagrams in the figures provide a visual representation of how the most notable variations appear precisely in these ions, in which two distinct categories of the GCBM and FWOR samples can also be recognized. As shown in Fig. 4a and c, the GCBM and FWOR samples exhibit similar variations in Na and Cl content, which correlates with TDI and EC variations. This observation highlights the role of halite-bearing components from the evaporate layers of cap rock (Gachsaran Formation) in contributing to the observed TDS in the studied GCBM samples. With the exception of Na and Cl, the concentrations of other major cations and anions declines from SO_4^{2-} to Ca^{2+} and Mg^{2+} (Fig. 4). Exceptionally, the SO_4^{2-} contents of sample S5 reach the highest (up to 11,000 mg/L, Table 2). The mean of Mg^{2+} content in GCBM-sampled springs is 315.7 mg/L, whereas it reaches 3600 mg/L in the FWOR-sampled wells (Fig. 4). GCBM from sampling point S3 shows decreasing SO_4^{2-} and increasing HCO_3^- concentrations for the dry season of the same year (Fig. 4b and d). Almost all major element concentrations underwent a drastic drop in W2. Considering that sample W2 in the FWOR group had ECs of 1576 µs/cm in the wet season and 2540 in the dry season, it is clear that this oil well has mixed with fresh karst waters at a depth of 2540 m.

The linear increase in the concentrations of Na^+ and Cl^- with TDI presents a similar origin for both ions in GCBM

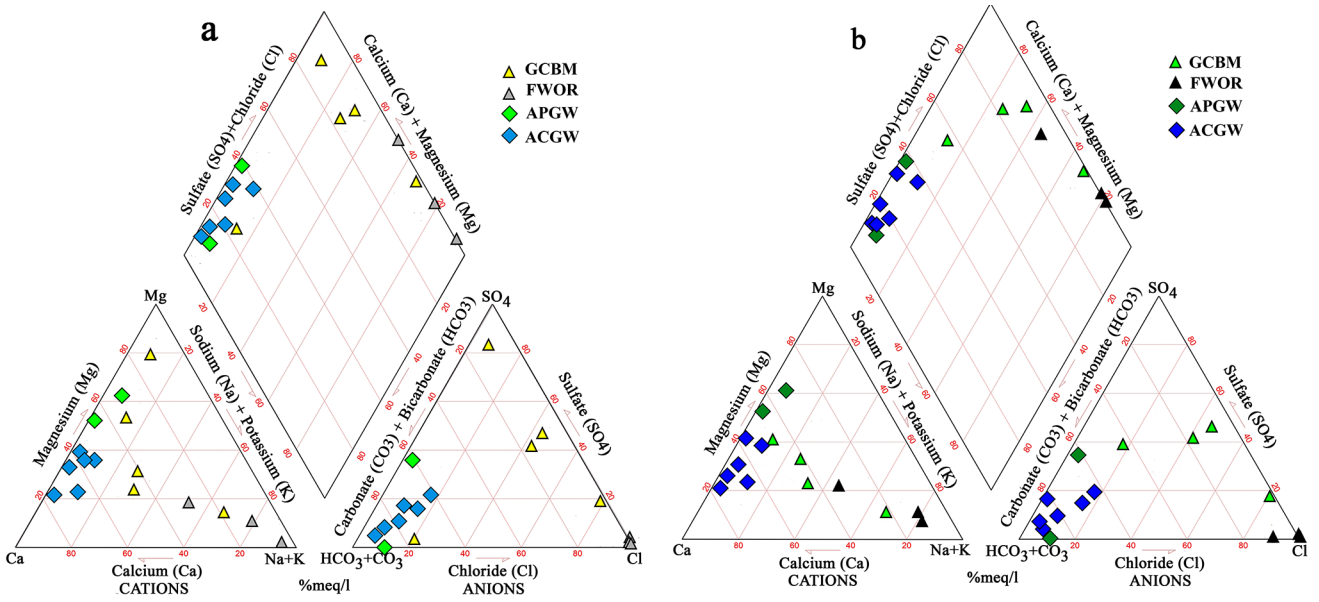

Fig. 3 Piper diagram of hydrochemical data from this study (GCBM, APGW, FWOR) and Farhadi et al. 2023 (ACGW) for (a) dry and (b) wet seasons

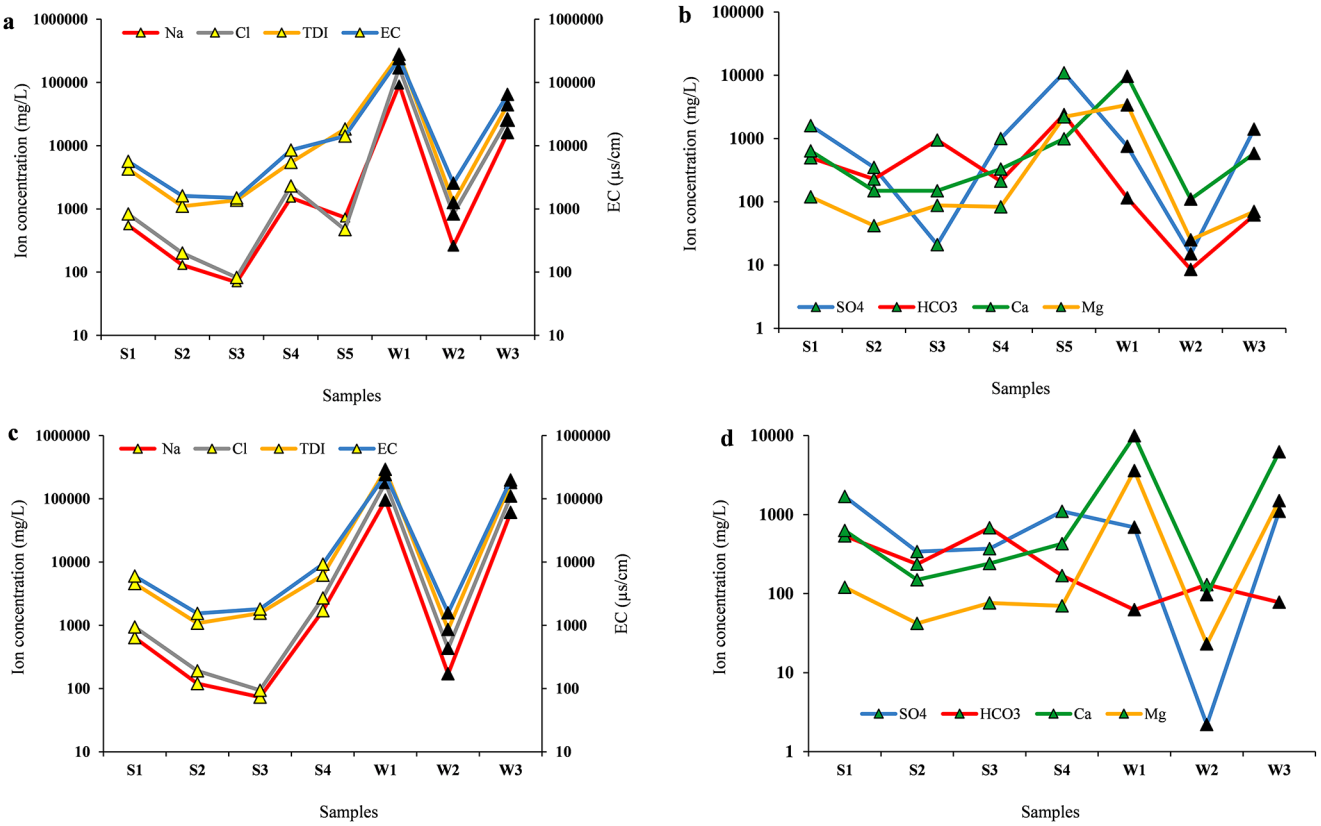

Fig. 4 Variation of major ions, TDI, and EC in GCBM and FWOR samples: (a) Na^+, Cl^-, EC, and TDI, and (b) SO_4^{2-}, HCO^-_3, Ca^{2+}, and Mg^{2+} in a dry season, and: (c) Na^+, Cl^-, EC, and TDI, and (d) SO_4^{2-}, HCO^-_3, Ca^{2+}, and Mg^{2+} in a wet season

and FWOR samples (Fig. 5a and b). The strong correlation between Ca^{2+}, Mg^{2+}, and SO_4^{2-} vs. TDI indicate the dissolution of gypsum and anhydrite in the GCBM samples of Gachsaran Formation as a reservoir of the bitumen mines (Fig. 5c and e, and 5f). In the GCBM samples, there is a positive relationship between TDI and all major ions except HCO_3^-, which shows discrepancies in its trend (Fig. 5d). Moreover, in the FWOR of the oil wells (Fig. 5d), the concentrations of HCO_3^- decreased with increasing TDI. As evident from Fig. 5, the TDI ratio to the major ions in ACGW is less than in GCBM. Moreover, APGW exhibits a similar behavior to ACGW.

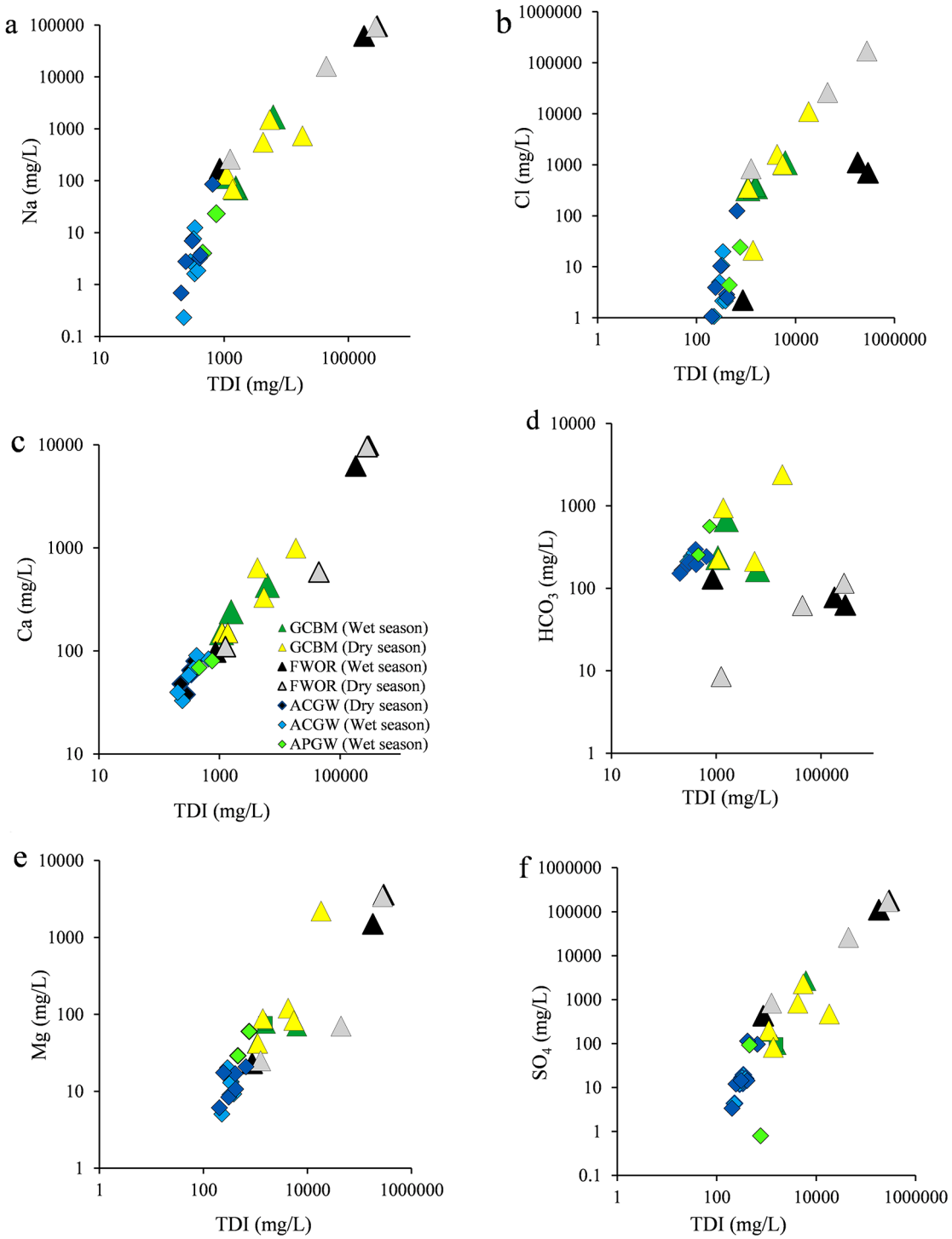

Fig. 5 The bivariate diagrams of major ions composition of the GCBM, APGW, ACGW, and FWOR samples; **a)** Na vs. TDI, **b)** Cl vs. TDI, **c)** Ca vs. TDI, **d)** HCO_3 vs. TDI, **e)** Mg vs. TDI, **f)** SO_4 vs. TDI

The chemical evolution of groundwater and water-rock interaction can be deduced by analyzing the relative proportions of cations and anions (Drever 1997). The Cl^- ion serves as a reference in this context due to its conservative nature in the process of freshwater mixing (Appelo and Postma 2005). Understanding salinization sources in water resources involves a crucial examination of the relationship between Cl^- vs. Na^+ (Mercado 1985). In this study, a Cl^- vs. Na^+ ionic ratio diagram was used to evaluate ion sources in the GCBM samples (Fig. 6a). A Na^+/Cl^- ratio equal to one indicates that halite is the source of these ions in water (Basins and Geo 2004). Deviation from unity suggests additional factors such as ion exchange processes, FWOR intrusion, and rock-water interaction. GCBM samples are

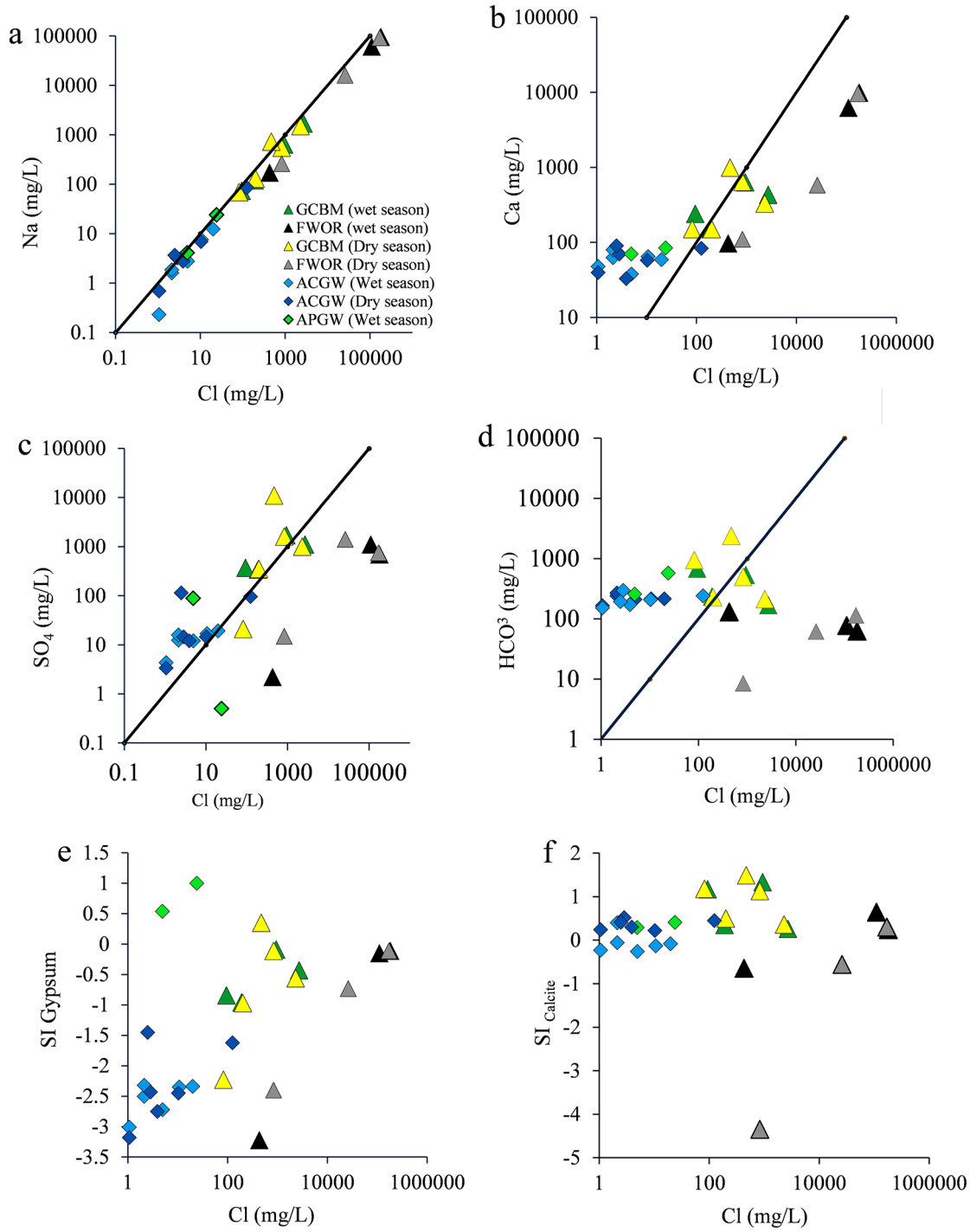

Fig. 6 Plots of Cl concentration vs.: (a) Na, (b) Ca, (c) SO_4, (d) HCO_3, (e) SI_{gypsum}, and (f) $SI_{calcite}$

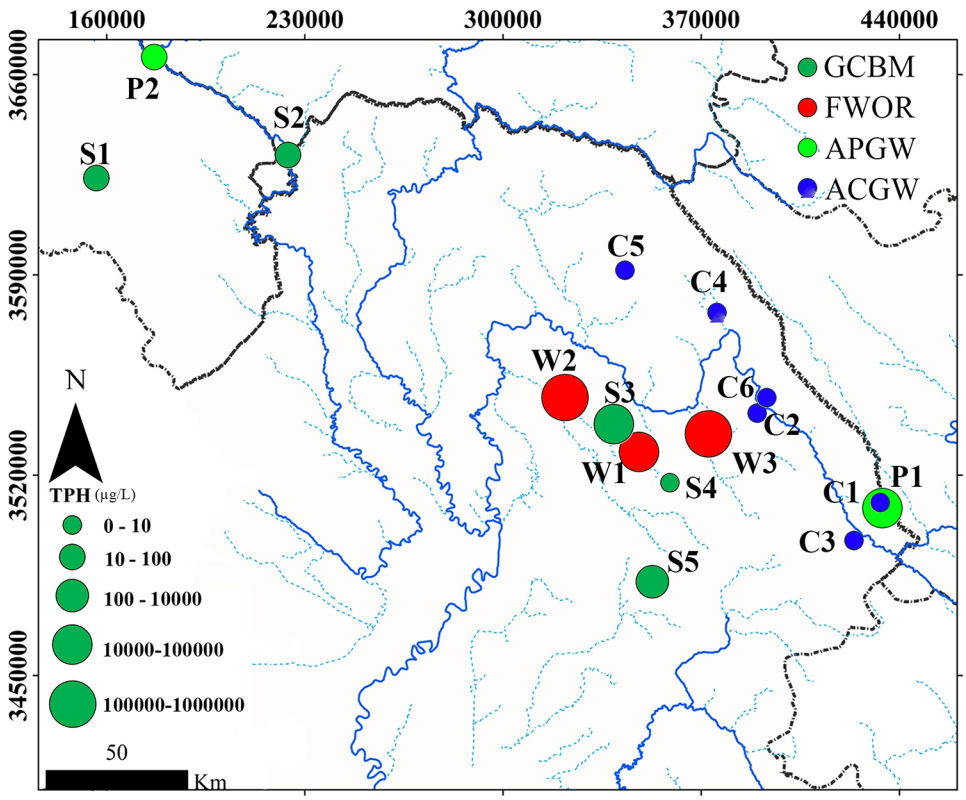

Fig. 7 Distribution of total petroleum hydrocarbon (TPH) in the GCBM, APGW samples, and FWOR samples of the oil wells

Table 4 TPH concentration in GCBM, APGW and FWOR in SW Iran

sample	S1	S2	S3	S4	S5	W1	W2	W3	P1	P2
TPH (µg/L)	40.2	26.3	19670.9	ND	2564	233629	33929.2	733880	1034.3	45

ND = Not Detected

scattered above the 1:1 line in the Ca^{2+} vs. Cl^{-} and HCO_3^{-} vs. Cl^{-} plots (Fig. 6b and d), indicating a departure from linearity between GCBM and FWOR, possibly due to processes modifying water chemistry. The Ca^{2+} enrichment could be affected by carbonate mineral dissolution. Similarly, in the SO_4^{2-} vs. Cl^{-} plot (Fig. 6c), ACGW, APGW, and some of the GCBM samples scatter above the 1:1 line, suggesting potential gypsum dissolution. To verify this, the saturation index (SI) of GCBM samples for gypsum and calcite was calculated, with some exceeding zero, indicating undersaturation, and the potential dissolution of gypsum minerals (Fig. 6). In contrast, the FWOR samples scatter below the 1:1 line. In Fig. 6d, some of the GCBM samples scatter above zero and are saturated with respect to calcite. This indicates that the chemical compositions of the GCBM are also affected by water-rock interactions.

Total Petroleum Hydrocarbon (TPH) Concentration

Crude oil and TPH pollutants are important contributors to environmental degradation due to their persistent characteristics and hydrophobic nature (Muthukumar et al. 2023). TPH concentration was measured in the GCBM and FWOR samples (Fig. 7). The total concentrations of TPH varied in GCBM samples from 26.3 to 19,670 µg/l, with an average concentration of 5575 µg/l. These findings were comparable to measurements taken at the FWOR of three oil wells, where the average TPH concentration was 333,813 µg/l (Table 4). Among the GCBM samples, S1, S2, S3, and S5 represent a high TPH concentrations and prompted concerns about the quality of groundwater impacts from bitumen exploration. The highest TPH concentration was recorded in sample S3, which was situated within an abandoned bitumen mine, and the groundwater discharge from the aquifer was minimal. The lowest TPH value was recorded in spring S4, which is located furthest from the bitumen mines. Moreover, the differences between GCBM and FWOR in S3 and S5 is low.

It is obvious that the TPH concentration values of GCBM and APGW samples greatly overlap. Three of the GCBM samples (S1, S2, and S4) contain lower TPH values than both of the APGW samples, with their TPH concentration values being of the order of the lower polluted APGW sample P2. Two of the GCBM samples have TPH concentrations greater than the APGW samples (S3, S5), with the concentration of

the higher polluted P1 sample being of the order of GCBM sample S5, while GCBM sample S3 far exceeds this. These concentrations far exceed the permissible limit set by WHO, which is 0.3 µg/L (WHO 2022), and display an unacceptable level of hydrocarbon contamination.

The Stable Isotopic Composition of the Waters

The stable isotopic compositions of the water samples are detailed in Table 2. The stable isotope compositions of GCBM exhibited $\delta^{18}O_{H2O}$ values ranging from −4.94 to -2.17‰ and $\delta^{2}H_{H2O}$ values ranging from −18.8 to -1.9‰. Meanwhile, the FWOR displayed significant variations, with $\delta^{18}O_{H2O}$ values ranging from −4.42 to +7.72‰ and $\delta^{2}H_{H2O}$ values ranging from −19.6 to +18.4‰. The relationships between $\delta^{18}O_{H2O}$ and $\delta^{2}H_{H2O}$ in different water sources are depicted in Fig. 8a. The S5 is a bitumen spring with $\delta^{2}H$ ranging from +27.7 to 51.8‰ V-SMOW and $\delta^{18}O$ ranging from +5 to 18.05‰ V-SMOW in Aug 2021 and Feb 2022.

The distribution of stable isotopes in both GCBM and FWOR (Fig. 8a) indicates that most of the samples are spread out on either side of the global meteoric water line (GMWL), defined by Craig (1961). This suggests that the primary source of GCBM is atmospheric precipitation. In contrast, FWOR samples distributed at the right of the GMWL line exhibit higher $\delta^{18}O_{H2O}$ and $\delta^{2}H_{H2O}$ values, except for the W2 sample. The W2 sample values clustered near the local meteoric water line (LMWL) and GMWL, and close to the GCBM samples (Fig. 8a).

The correlation between ion composition, specifically Cl^{-}, and isotopes ($\delta^{18}O$) in groundwater reveals the influence of various processes on salt enrichment (Qian et al. 2014; Parvaiz et al. 2021). The relationship between Cl^{-} and $\delta^{18}O$ in GCBM is depicted in Fig. 8b. A notable positive correlation was identified between $\delta^{18}O$ and Cl^{-} in GCBM salinity enrichment attributed to bitumen mining. Two distinct trends emerged: (1) an increase in Cl^{-} content coincided with an increase in the $\delta^{18}O$ values in GCBM; (2) in FWOR, the Cl^{-} content remained relatively stable despite an increase in the $\delta^{18}O$ values.

In the first trend, there was a slight increase in $\delta^{18}O$ values with an accompanying increase in Cl^{-} content in GCBM. The extensive distribution of bitumen mines in the study area led to bitumen leaching, altering the isotopic composition of GCBM and slightly enriching $\delta^{18}O$, particularly in S5. The GCBM samples, S1 and S3, along with bitumen drainage, exhibited similar $\delta^{18}O$ values and Cl^{-} content during both dry and wet seasons (Fig. 8b). The proximity of bitumen mining markedly influenced the isotopic and chloride compositions of GCBM in this region. Sample S5, located near the abandoned Mamatin bitumen mine, had a high EC (14,140 µs/cm) because it comes out of an evaporite layer of

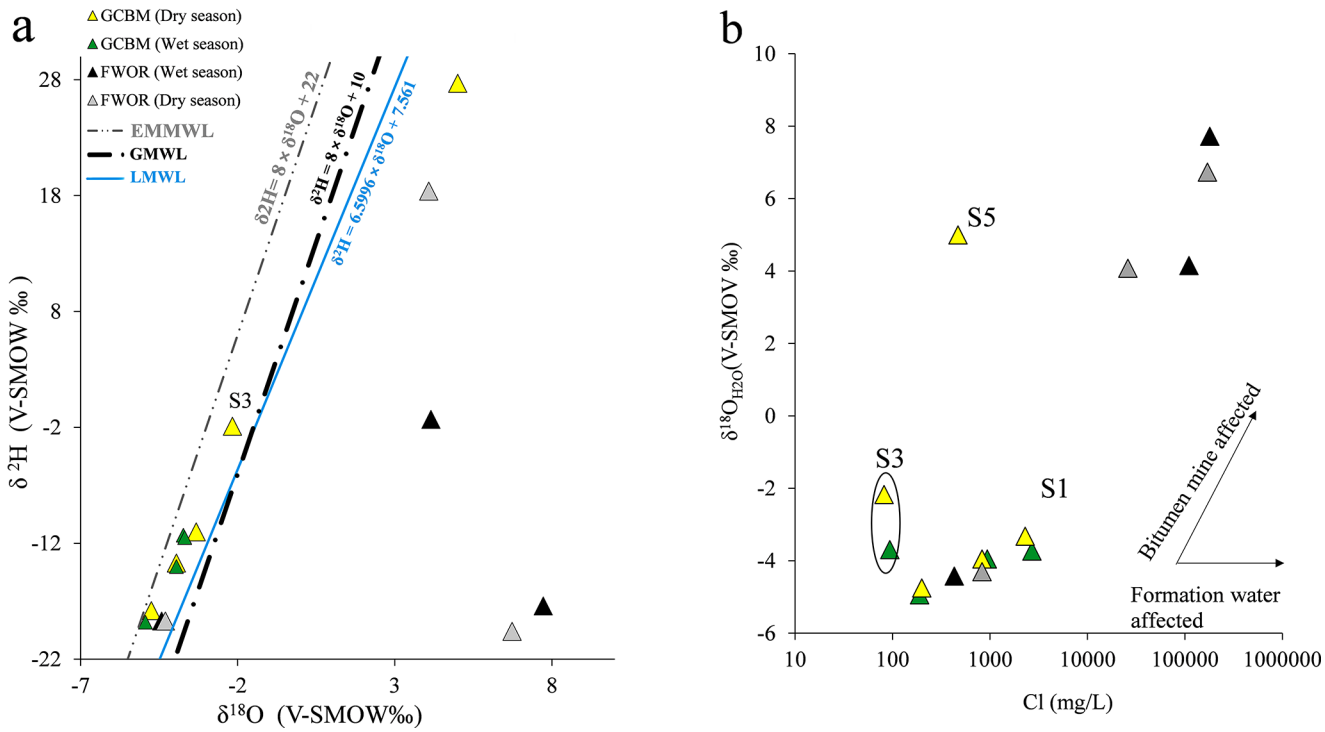

Fig. 8 (a) Plot of δ^{18}OH2O vs. δ^{2}HH2O for the waters in the study area, featuring the global meteoric water line (GMWL) established by Craig in 1961 and the local meteoric water line (LMWL) by Farhadi et al. (2020), (b) δ18OH2O vs. Cl concentration

gypsum. According to the isotopic analysis results, it is very possible that this sample was mixed with FWOR.

Discussion

The graphs in Fig. 4 depict fluctuations in chemical concentrations and other parameters, such as pH and EC, in GCBM and FWOR during both dry and wet seasons. Based on Fig. 6, a comparison was made between GCBM and FWOR. The graph shows a decreasing trend in Ca^{2+}/Cl^-, HCO_3^-/Cl^-, SI calcite/Cl^-, and SI gypsum/Cl^- for GCBM, while an increasing trend was observed for the FWOR samples. In the SO_4^{2-}/Cl^- graph, GCBM samples exhibit an increasing trend, whereas FWOR samples show a decreasing trend.

As depicted in Fig. 6, the results reveal a high levels of Cl^- in GCBM samples from bitumen mines. The concentrations of Cl^- and Na^+ exhibit a positive correlation (Fig. 6a), resulting in a Na^+/Cl^- ratio of 0.69 in GCBM and 0.49 in FWOR close to deep water (Aquilina et al. 2002). The salinity of the GCBM samples is attributed to halite dissolution from the Gachsaran evaporites. Considering the impact of bitumen mining on groundwater and the Na^+/Cl^- ratio, it is evident that bitumen mines contribute to groundwater salinity. The presence of minerals and their reactivity in groundwater was further explored using PHREEQC modeling, specifically examining saturation indices. The Ca^{2+}/Cl^- and SO_4^{2-}/Cl^- ratios of GCBM samples fall below the 1:1 line, potentially influenced by inputs from bitumen mining. A saturation index > 0.5 indicates supersaturation of minerals concerning GCBM, and vice versa. The saturation indices of gypsum and calcite, plotted against Cl^-, reveal a prevalent trend of supersaturation in most of the samples (Fig. 6e and f). This prevailing supersaturation in GCBM elucidates the decline in Cl^- levels and can be attributed to extensive mineral dissolution caused by bitumen mining in the study area. The dissolution of gypsum and calcite contributes to increased concentrations of Ca^{2+}, SO_4^{2-}, Mg^{2+}, HCO_3^-, and Cl^- in GCBM (Su et al. 2020).

The results (Fig. 7) indicate that the GCBM samples had a high level of TPH (max. 19,670 µg/L). The spatial distribution map of TPH (Fig. 7) illustrates that high concentrations of TPH occurred in most GCBM samples within the study area, indicating that the high TPH in these samples was due to bitumen. As shown in Fig. 8, GCBM samples were enriched in $\delta^{18}O$ and δ^2H, and sample S3 had a positive amount of $\delta^{18}O$. In FWOR, evaporation can be ruled out because of the depth of the FWOR samples. Furthermore, the Cl^- vs. $\delta^{18}O$ plots (Fig. 8b) suggest that groundwater chemistry is influenced by mining and mineral dissolution.

Conclusions

Based on the hydrochemistry and isotopic characteristics of the groundwater contaminated by abandoned bitumen mines (GCBM) in southwest Iran, bitumen seepage is contributing to groundwater contamination. Groundwater samples associated with the abandoned bitumen mines in the study area are affected mainly by the gypsum layers in the Cap Rock formation of the hydrocarbon reservoirs. The most prevalent dissolved cation and anions in the GCBM were $Mg^{2+} > Na^+ > Ca^{2+} > K^+$ and $SO_4^{2-} > Cl^- > HCO_3^-$. These ions are the main contributors to the TDI concentrations. Dissolution of carbonate, gypsum, and/or anhydrite and halite control the hydrochemical processes in the carbonate-evaporate aquifers. According to the $\delta^{18}O_{H2O}$ and δ^2H_{H2O} diagrams, the enrichment of the GCBM samples suggest that they originated from local meteoric water and were affected by the bitumen mines. The total concentration of TPH in the GCBM samples ranged from 26.3 to 19,670 µg/L. The karst aquifer pollution resulting from the abandoned bitumen mines in southwest Iran occasionally exceed the geogenic pollution from natural bitumen deposits by more than an order of magnitude. Generally, however, pollution from these mines stays within orders of magnitude of the geogenic pollution. Graphical biplots identified mineral dissolution, evaporation, and input of bitumen as the primary sources of groundwater salinity.

Acknowledgements The authors thank Shahid Beheshti University of Iran for partial financial support (grants for Ph.D. and sabbatical leave), Dr. Florian Eichinger managing director of Hydroisotop GmbH Co. for providing laboratory space, Dr. Andrei Voropaev for providing analytical support, and Janet Wohlgemuth for her help with isotope analysis.

References

Abdelfatah E, Berton P, Rogers R, Bryant S (2018) Low-temperature bitumen recovery from oil sand reservoirs using ionic liquids. DOI. https://doi.org/10.2118/193673-MS

Abu-alnaeem MF, Yusoff I, Ng TF, Alias Y, Raksmey M (2018) Assessment of groundwater salinity and quality in Gaza coastal aquifer, Gaza Strip, Palestine: an integrated statistical, geostatistical and hydrogeochemical approaches study. Sci Total Environ 615:972–989. https://doi.org/10.1016/j.scitotenv.2017.09.320

Adeyemi GO, Akinmosin AA, Aladesanmi AO, Badmus GO (2013) Geophysical and sedimentological characterization o f a tar sand rich area in south-western Nigeria. J Environ Earth Sci 3(14):71–83

Alberta Biodiversity Monitoring Institute (2018) Oil Sands Region Oil Sands Regions [WWW Document]. Alberta Biodiversity Monitoring Institute. URL. https://abmi.ca/home/reports/2020/human-footprint/details.html?id=19. (Accessed 22 January 2022)

Alberta Energy Regulator (2021) Alberta Energy Outlook 2021 (statistical no. ST 98). Alberta Energy Regulator, Calgary, Alberta

Ameri M, Mansourian A, Ashani SS, Yadollahi G (2011) Technical study on the Iranian gilsonite as an additive for modification of asphalt binders used in pavement construction. Constr Build Mater 25:1379–1387. https://doi.org/10.1016/j.conbuildmat.2010.09

Appelo CAJ, Postma D (2005) Geochemistry, Groundwater and Pollution. A.A. Balkema, Leiden, The Netherlands

Attanasi ED, Meyer RF (2010) Natural bitumen and extra-heavy oil. Surv Energy Resour 22:123–140

Bahroudi A, Koyi HA (2004) Tectono-sedimentary framework of the Gachsaran formation in the Zagros foreland basin. Mar Pet Geol 21:1295–1310. https://doi.org/10.1016/j.marpetgeo.2004.09.0

Barnes CJ, Allison GB (1988) Tracing of water movement in the unsaturated zone using stable isotopes of hydrogen and oxygen. J Hydrol 100:143–176. https://doi.org/10.1016/0022-1694(88)90184-9

Berberian M, King GCP (1981) Towards a paleogeography and tectonic evolution of Iran. 701 Can J Earth Sci 18:210–265

Bordenave ML, Burwood R (1995) The albian Kazhdumi formation of the Dezful Embayment, Iran: one of the most efficient petroleum generating systems. In: Katz BJ (ed) Petroleum Source Rocks, casebooks in Earth sciences. Springer, Berlin, Heidelberg, pp 183–207

Brown LD, Ulrich AC (2015) Oil sands naphthenic acids: a review of properties, measurement, and treatment. Chemosphere 127:276–290. https://doi.org/10.1016/j.chemosphere.2015.02.003

Brown DM, Bonte M, Gill R, Dawick J, Boogaard PJ (2017) Heavy hydrocarbon fate and transport in the environment. Q J Eng Geol Hydrogeol 50:333–346. https://doi.org/10.1144/qjegh2016-142

Craig H (1961) Isotopic variations in meteoric waters. Science 133:1702

Dickey PA (1966) Patterns of chemical composition in deep subsurface waters. AAPG Bull 50:2472–2478

Drever JI (1997) The Geochemistry of Natural Waters: Surface and Groundwater Environments. Prentice-Hall, NJ, USA

Farhadi S, Alijani F, Nassery HR (2020) Characteristics of stable isotopes of the heavy rainfall event of April 2019 in Southwest Iran comparing with LMWL of other regions of country and neighboring countries. J Agric Meteorol 8:44–59 (in Persian). https://doi.org/10.22125/agmj.2020.223190.1093

Farhadi S, Alijani F, Nassery HR, Daneshian S (2023) Comparison of hydrogeochemistry and hydrogeology of Asmari and Sarvak formations as a reservoir of large karst springs of Zagros in northeast of Khuzestan. J Hydrogeol 7:143–159 (in Persian). https://doi.org/10.22034/HYDRO.2023.14136

Finkel ML (2018) The impact of oil sands on the environment and health. Curr Opin Environ Sci 3:52–55. https://doi.org/10.1016/j.coesh.2018.05.002

Gosselin P, Hrudey SE, Naeth MA, Plourde A, Therrien R, Van Der Kraak G, Xu Z (2010) Environmental and Health Impacts of Canada's Oil Sands Industry - Scientific Report (Scientific Report). The Royal Society of Canada

Ismail MJ, Ettensohn FR, Handhal AM, Al-Abadi A (2021) Facies analysis of the middle cretaceous Mishrif formation in southern Iraq borehole image logs and core thin-sections as a tool. Mar Pet Geol 133:105324. https://doi.org/10.1016/j.marpetgeo.2021.105324

Kelly EN, Schindler DW, Hodson PV, Short JW, Radmanovich R, Nielsen CC (2010) Oil sands development contributes elements toxic at low concentrations to the Athabasca River and its tributaries. Proc Natl Acad Sci U SA 107:16178–16183. https://doi.org/10.1073/pnas.1008754107

Korosi JB, Cooke CA, Eickmeyer DC, Kimpe LE, Blais JM (2016) In - situ bitumen extraction associated with increased petrogenic polycyclic aromatic compounds in lake sediments from the Cold Lake heavy oil fields (Alberta, Canada). Environ Pollut 218:915–922. https://doi.org/10.1016/j.envpol.2016.08.032

Li X, Wu P, Han Z, Zha X, Ye H, Qin Y (2017) Effects of mining activities on evolution of water quality of karst waters in Midwestern Guizhou, China: evidences from hydrochemistry and isotopic composition. Environ Sci Pollut Res 25:1220–1230. https://doi.org/10.1007/s11356-017-0488-y

Maadanara consulting engineering (1996) Investigation of gilsonite mines in Kermanshah and Ilam provinces. Geological survey of Iran, Technical report

Maadankave consulting engineering (1999) Investigation of gilsonite mines in Lorestan province. geological survey of Iran, Technical report

Mehrabi H, Yahyaei E, Navidtalab A, Rahimpour-Bonab H, Abbasi R, Omidvar M, Assadi A, Honarmand J (2023) Depositional and diagenetic controls on reservoir properties along the shallow-marine carbonates of the Sarvak formation, Zagros Basin: petrographic, petrophysical, and geochemical evidence. Sediment Geol 454:106457. https://doi.org/10.1016/j.sedgeo.2023.106457

Muthukumar B, Surya S, Sivakumar K, AlSalhi MS, Rao TN, Devanesan S, Arunkumar P, Rajasekar A (2023) Influence of bioaugmentation in crude oil contaminated soil by Pseudomonas species on the removal of total petroleum hydrocarbon. Chemosphere 310:136826. https://doi.org/10.1016/j.chemosphere.2022.136826

Noorian Y, Moussavi-Harami R, Hollis C, Reijmer JJG, Mahboubi A, Omidpour A (2022) Control of climate, sea-level fluctuations and tectonics on the pervasive dolomitization and porosity evolution of the Oligo-Miocene Asmari formation (Dezful Embayment, SW Iran). Sedimet Geol 427:106048. https://doi.org/10.1016/j.sedgeo.2021.106048

Ola PS, Olabode SO (2017) Tar sand occurrence: implications on hydrocarbon exploration in the offshore Benin Basin. Petrol Sci Technol 35:523–534. https://doi.org/10.1080/10916466.2016.1265560

Parvaiz A, Khattak JA, Hussain I, Masood N, Javed T, Farooqi A (2021) Salinity enrichment, sources and its contribution to elevated groundwater arsenic and fluoride levels in Rachna Doab, Punjab Pakistan: stable isotope (δ^2H and $\delta^{18}O$) approach as an evidence. Environ Pollut 268:115710. https://doi.org/10.1016/j.envpol.2020.115710

Piper AM (1944) A graphic procedure in the geochemical interpretation of water analysis. EOC trans. Am Geophyis Onion 25:914–928. https://doi.org/10.1029/TR025i006p00914

Qian H, Wu J, Zhou Y, Li P (2014) Stable oxygen and hydrogen isotopes as indicators of lake water recharge and evaporation in the lakes of the Yinchuan Plain. Hydrol Process 28:3554–3562. https://doi.org/10.1002/hyp.9915

Rahimi E, Shekarian Y, Mastri Farahani S, Asgari GR, Nakini A (2020) New approach in application of the AHP–Fuzzy TOPSIS method in mineral potential mapping of the natural bitumen (gilsonite): a case study from the Gilan-e-Gharb Block, the Kermanshah, west of Iran. Am J Appl Sci 13(1):96–110. https://doi.org/10.3844/ajeassp.2020.96.110

Sherkati S, Letouzey J, Lamotte DFD (2006) Central Zagros fold-thrust belt (Iran): new insights from seismic data, field observation, and sandbox modeling. Tectonics 25:1–27

Speight JG (2005) Natural bitumen (tar sands) and heavy oil. Coal, Oil Shale, Nat Bitumen, Heavy Oil, Peat, Encyclopedia of Life Support Systems (Vol. II, 141)

Stöcklin J (1968) Salt deposits of the Middle East. In: Mattox RB (Ed.), Saline deposits: a symposium based on papers from the International Conference on Saline Deposits. Geological Society of America, Special Paper 88. Houston, Texas

Stoyanovich SS, Yang Z, Hanson M, Hollebone BP, Orihel DM, Palace V (2019) Simulating a spill of diluted bitumen: environmental weathering and submergence in a model freshwater system. Environ Toxicol Chem 38:2621–2628. https://doi.org/10.1002/etc.4600

Tiwari AK, Singh AK (2014) Hydrogeochemical investigation and groundwater quality assessment of Pratapgarh district, Uttar

Pradesh. J Geol Soc India 83:329–343. https://doi.org/10.1007/s12594-014-0045-y

Tiwari AK, Pisciotta A, Maio MD (2019) Evaluation of groundwater salinization and pollution level on Favignana Island, Italy. Environ Pollut. 249:969–981. https://doi.org/10.1016/j.envpol.2019.03.016

Vander Meulen IJ, Schock DM, Akhter F, Mundy L, Eccles KM, Soos C, Peru KM, McMartin DW, Headley J, Pauli BD (2023) Site-specific spatiotemporal occurrence and molecular congener distributions of naphthenic acids in Athabasca oil sands wetlands of Alberta, Canada. Environ Pollut 333:122061. https://doi.org/10.1016/j.envpol.2023.122061

Wasiuta V, Kirk JL, Chambers PA, Alexander AC, Wyatt FR, Rooney RC, Cooke CA (2019) Accumulating mercury and methylmercury burdens in watersheds impacted by oil sands pollution. Environ Sci Technol 53:12856–12864. https://doi.org/10.1021/acs.est.9b02373

White DE (1957) Magmatic, connate and meteoric waters. Geol Soc Am Bull 68:1659–1682

WHO (World Health Organization) (2022) Guidelines for drinking-water quality: Fourth edition incorporating the first and second addenda. https://www.who.int/publications/i/item/9789240045064

Zhang X, Li X, Gao X (2016) Hydrochemistry and coal mining activity induced karst water quality degradation in the Niangziguan karst water system, China. Environ Sci Pollut Res 23:6286–6299. https://doi.org/10.1007/s11356-015-5838-z

Zhang M, Chen L, Yao D, Hou X, Zhang J, Qin H, Ren X, Zheng X (2022a) Hydrogeochemical processes and inverse modeling for a multilayer aquifer system in the Yuaner Coal Mine, Huaibei Coalfield, China. Mine Water Environ 41:775–789. https://doi.org/10.1007/s10230-022-00851-0

Zhang J, Chen L, Hou X, Ren X, Li J, Chen (2022b) Hydrogeochemical processes of Carboniferous limestone groundwater in the Yangzhuang Coal Mine, Huaibei Coalfield, China. Mine Water Environ 41:504–517. https://doi.org/10.1007/s10230-022-00861-y